REPORT DOCUMENTATION PAGE

AFRL-SR-AR-TR-02-

0850

1. AGENCY USE ONLY *(Leave blank)*

2. REPORT DATE

3. REPORT TYPE AND DATES COVERED

4/15/2000 to 4/14/2001 Final

4. TITLE AND SUBTITLE

(DURIP 00) Advanced High Frequency Communication and Optoelectronic Radar Systems

5. FUNDING NUMBERS

61103D
3484/US

6. AUTHOR(S)

Professor Fetterman

7. PERFORMING ORGANIZATION NAME(S) AND ADDRESS(ES)

Univ of California
1401 Ueberroth Bldg
Box 951406
Los Angeles CA 90095-1406

8. PERFORMING ORGANIZATION REPORT NUMBER

9. SPONSORING/MONITORING AGENCY NAME(S) AND ADDRESS(ES)

Department of the Air Force
Air Force Office of Sdentific Research
801 N. Randolph St Rm 732
Arlington. VA 22203-1977

10. SPONSORING/MONITORING AGENCY REPORT NUMBER

F49620-00-1-0287

11. SUPPLEMENTARY NOTES

12a. DISTRIBUTION AVAILABILITY STATEMENT

Distribution Statement A. Approved for public release; distribution is unlimited.

12b. DISTRIBUTION CODE

13. ABSTRACT *(Maximum 200 words)*

We have demonstrated photonic time-stretching (PTS) of radio frequency (RF) signals using our novel polymer modulators and two techniques to reduce the power penalty from the effects of fiber chromatic dispersion. A Single-sideband (SSB) modulator configuration has almost eliminated the effect of this penalty without bandwidth limitations. The double-sideband (DSB) modulator configuration, with an alternative quadrature bias point, has also shown significant improvement of bandwidth limitations for a given fiber link length. In addition, we have investigated the general characteristics of the power penalty's relation with several modulation schemes.

20021126 090

14. SUBJECT TERMS

15. NUMBER OF PAGES

16. PRICE CODE

17. SECURITY CLASSIFICATION OF REPORT	18. SECURITY CLASSIFICATION OF THIS PAGE	19. SECURITY CLASSIFICATION OF ABSTRACT	20. LIMITATION OF ABSTRACT
Unclassified	Unclassified	Unclassified	UL

Standard Form 298 (Rev. 2-89) (EG)
Prescribed by ANSI Std. 239.18
Designed using Perform Pro, WHS/DIOR, Oct 94

Final Performance Report

Advanced High Frequency Communications and Optoelectronic Radar Systems

F49620-00-1-0287

Jul 15 2001

During the period of this contract we established a tunable Femtosecond Laser capability. This unit combined a Ti:Sapphire laser Laser with a Parametric Oscillator. This along with a 50 GHz DURIP sampling oscilloscope permitted us to make precise measurements on time scales that were previously severely limited.

As an example of the use of the high speed oscilloscope I enclose our first paper on Photonic Oscillators. The Photonic Time Stretching is a another area of study and I enclose the original and the latest version.

Several experiments are currently in progress using this Femtosecond facility and Sampling scopes and Optical Amplifiers.. In one of them we have looked at the use of our ultra fast modulators as a function of wavelength. This has then permitted us to understand the effects of path length mismatches in the two arms of the M.Z. for pulsed signals.

In a second set of measurements we a now able to use electrooptic switches in determining the highest modulation speeds of our traveling wave modulators. This experiment had been attempted with lower powers without success. The instrumentation grant has therefor dramatically increased our experimental capabilities in the high speed regime.

Photonic Time-Stretching with Reduction of Fiber Chromatic Dispersion Effects Using Polymer Modulators

Jeehoon Han, Byoungjoon Seo, Yan Han, Bahram Jalali and Harold Fetterman
Electrical Engineering Department, UCLA, Los Angeles, CA 90095

ABSTRACT

We have demonstrated photonic time-stretching (PTS) of radio frequency (RF) signals using our novel polymer modulators and two techniques to reduce the power penalty from the effects of fiber chromatic dispersion. A Single-sideband (SSB) modulator configuration has almost eliminated the effect of this penalty without bandwidth limitations. The double-sideband (DSB) modulator configuration, with an alternative quadrature bias point, has also shown significant improvement of bandwidth limitations for a given fiber link length. In addition, we have investigated the general characteristics of the power penalty's relation with several modulation schemes.

I. INTRODUCTION

PTS utilizes optical systems to enable high-speed analog-to-digital conversion (ADC) of RF signals at otherwise inaccessible high frequencies. By exploiting chirped optical pulses and chromatic dispersion in standard optical fibers, high-frequency RF signals can be stretched in time without distortion to lower frequency regimes. At these lower frequencies conventional electronic ADC's are able to digitize with high resolution [1].

In a previous work, we successfully demonstrated PTS system at very high frequencies up to 102 GHz, which was enabled by the high frequency performance of our polymer modulators [2]. However, as in conventional photonic links using CW lasers, the

actual bandwidth of PTS system associated with DSB modulation is also limited by inherent fiber chromatic dispersion effects [1], [2]. This paper describes the general theory and experiment to reduce this power penalty in both continuous wave (CW) sources and PTS system using DSB and SSB modulators. These devices are based on a new EO polymer material, CPW1/APC and employ our state-of-the-art polymer modulator technology [3].

II. POWER PENALTY WITH CW SOURCE

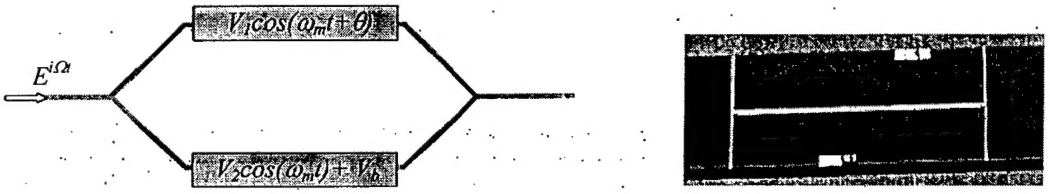

Fig.1 The general schematic for MZM structure representing all possible modulation schemes and bias points and a device fabricated with polymer material, CPW1/APC

The simplest and best technique to modulate optical field with RF signal is an intensity modulation scheme via Mach-Zehnder modulators (MZM). The schematic drawing for MZM is shown in Fig. 1 representing all possible modulation schemes and bias points. If the input optical signal at Ω is $E_{in}(t)=e^{i\Omega t}$ with unit amplitude, the generalized expression for output optical field from MZM modulated at ω_m is given by,

$$E(t)=\frac{1}{2}e^{i\Omega t}\{e^{i\Delta_1\cos(\omega_m t+\theta)}+e^{i\Delta_2\cos(\omega_m t)+i\phi_b}\} \quad (1)$$

where $\Delta_i=\pi\cdot V_i/V_\pi$ is the modulation depth at i arm, $\phi_b=\pi\cdot V_b/V_\pi$ is the optical phase shift controlled by a DC bias, V_π is the half-wave voltage. When this signal travels through the standard fiber with length of L, the resulting optical field can be written in

terms of three frequency components, Ω, $\Omega-\omega$ and $\Omega+\omega$, with different phase changes due to the chromatic dispersion.

$$E(t) = \frac{1}{2}\{[J_0(\Delta_1) + J_0(\Delta_2)e^{i\delta}]e^{i\Omega t}e^{i\varphi_\Omega} + i[J_0(\Delta_1)e^{i\theta} + J_0(\Delta_2)e^{i\delta}]e^{i(\Omega-\omega_m)}e^{i\varphi_{\Omega-\omega_m}} + i[J_0(\Delta_1)e^{i\theta} + J_0(\Delta_2)e^{i\delta}]e^{i(\Omega+\omega_m)}e^{i\varphi_{\Omega+\omega_m}}\} \quad (2)$$

where $J_0(\Delta_1)$, $J_0(\Delta_2)$, $J_1(\Delta_1)$ $J_1(\Delta_2)$ are the Bessel function values. Each phase change can be specified by usual Taylor expansion of the propagation constants $\beta(\omega)$:

$$\begin{aligned} \varphi_\Omega &= \beta(\Omega)L \\ \varphi_{\Omega-\omega_m} &= \beta(\Omega)L - \beta'(\Omega)L\omega_m + \frac{1}{2}\beta''(\Omega)L\omega_m^2 \\ \varphi_{\Omega+\omega_m} &= \beta(\Omega)L + \beta'(\Omega)L\omega_m + \frac{1}{2}\beta''(\Omega)L\omega_m^2 \end{aligned} \quad (3)$$

where group velocity dispersion in standard fibers is $|D_\lambda| \equiv \frac{2\pi c}{\lambda_0^2}\beta'' = 17$ ps/km·nm

At the photodiode, a single component at the modulation frequency is produced as a result of interference among these components. Normally the detected RF power is associate with their phase relationship, which consequently is a strong function of dispersion parameter, fiber length and modulation frequency as can be seen in (3). In the following sections, it will be discussed how it also could be affected much by the modulation schemes and bias conditions.

a) DSB modulation with push-pull operation ($\Delta_1 = \Delta_2 = \Delta$, $\theta = 0$)

Here both arms are driven by the RF signal with equal power and the same phase. One arm is biased with $V_{\pm b}$ corresponding to the quadrature voltage on the positive and negative slope of the MZM transfer function such that $\phi_{+b} = \pi V_{+b}/V_\pi = \pi/2$, $\phi_{-b} = \pi V_{-b}/V_\pi = -\pi/2$ with respect to the other arm. This is so called push-pull operation and the optical field from the MZM can be expressed by

$$E(t) = \frac{1}{2} e^{i\Omega t} \{ e^{i\Delta \cos(\omega_m t)} \pm i e^{i\Delta \cos(\omega_m t)} \} \tag{4}$$

The resulting intensity at the modulation frequency after propagating through fiber L is

$$I_{\omega_m}(t) = 2 J_0 J_1 \sin(\omega_m t - \beta' L \omega_m) \cos(\frac{\beta'' L \omega_m{}^2}{2}) \tag{5}$$

An optical carrier and two sidebands generated by DSB modulation experience different phase shifts along the fiber and result in relative phase difference between the carrier and each sideband. Due to this effect, the RF power detected at the modulation frequency is not constant but varying with their phase relationship which is dependent on the dispersion parameters, fiber length, and modulation frequency. This power penalty is represented by the second cosine term in (5). Since, in this case, both RF arms are balanced, there is no initial phase difference between carrier and each sideband at the MZM so that the power variation appears in a single form of $\cos(\frac{\beta'' L \omega_m{}^2}{2})$ regardless of bias point.

b) DSB modulation driven with only single-arm ($\Delta_1 = 0$, $\Delta_2 = \Delta$)

When only one of arms is modulated with bias voltages $V_{\pm b}$, the optical field from the MZM can be expressed by

$$E(t) = \frac{1}{2} e^{i\Omega t} \{ 1 \pm i e^{i\Delta \cos(\omega_m t)} \} \tag{6}$$

The resulting intensity at ω_m after propagating through fiber a distance L is

$$I_{\omega_m}(t) = 2\sqrt{2} J_0 J_1 \sin(\omega_m t - \beta' L \omega_m) \cos(\frac{\beta'' L \omega_m{}^2}{2} \pm \frac{\pi}{4}) \tag{7}$$

Similarly to the previous push-pull operation case, the detected RF power is varying with a cosine function due to the same effect. However, in this case, this modulation scheme introduces the additional phase difference between the carrier and each sideband at the MZM, which influences on the detected RF power. As shown in (7), the second cosine term is shifted by amount of $\pm\pi/4$ where the signs are corresponding to bias voltages, $V_{\pm b}$. This indicates that the first power null for each bias point, when the second cosine term is zero, appears at different modulation frequencies (or fiber length). So, DSB modulation driven by only one arm and biased at V_{-b} can increase the bandwidth for a given fiber link length or vice versa.

Fig. 2 shows the theoretical graph for the power penalty as a function of modulation frequencies resulting from two DSB modulation schemes discussed above. Push-pull operation has only one power null while single-arm operation has two depending on the bias points. It can be also seen that the bandwidth of single-arm operation biased with V_{-b} increased compared to other two cases.

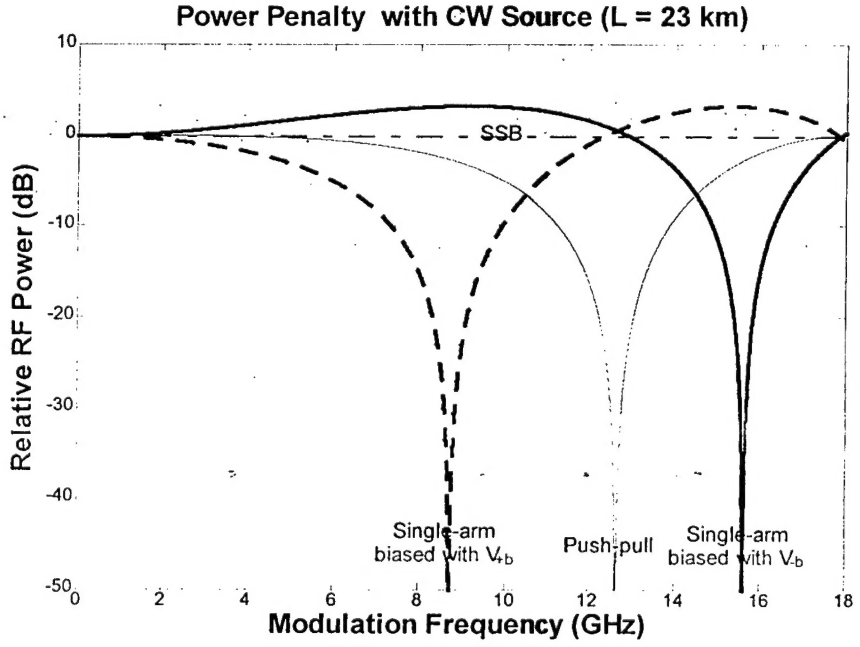

Fig.2 Power penalty as a function of modulation frequencies in CW case with different modulation schemes and bias points for fiber length of 23 km

c) SSB modulation ($\Delta_1 = \Delta_2 = \Delta$, $\theta = \pm\pi/2$)

When the both arms are modulated but RF phase difference on two arms is $\pm\pi/2$, with bias voltage $V_{\pm b}$, the optical field from the MZM becomes

$$E(t) = \frac{1}{2} e^{i\Omega t} \{ e^{\mp i\Delta \sin(\omega_m t)} \pm i e^{i\Delta \cos(\omega_m t)} \} \tag{8}$$

The resulting intensity at ω_m after propagating through fiber a distance L is

$$I_{\omega_m}(t) = 2\sqrt{2} J_0 J_1 \cos(\omega_m t - \beta' L \omega_m + \frac{\pi}{4}) \tag{9}$$

SSB modulation cancels out one of sidebands and generates a carrier and only one sideband. As a consequence, it is seen in (9) that the second cosine term associated with power penalty is dropped and the detected RF power is constant. Ideally, the RF signal generated by SSB modulation does not suffer from bandwidth or fiber link length (Fig. 2).

III. POWER PENALTY IN TIME-STRETCHING SYSTEM

Time stretching exploits group velocity dispersion to temporally expand a pulse while preserving its envelope shape which has information. The details of this theory are in papers [1] and [2]. Instead of the plane waveform in the CW case, a transform limited Gaussian pulse is assumed such as

$$E_{source}(t) = \exp(-\frac{t^2}{\tau^2}) \exp(i\Omega t) \tag{10}$$

Then, the same principles as in the CW case are applied to the PTS system so that the resulting intensity at ω_m for each modulation scheme is

$$I_{\omega_m}(t) \propto \cos\left(\frac{\beta'' L_2 \omega_m^{\,2}}{2M}\right) : \text{DSB push-pull operation with } V_{\pm b} \tag{11}$$

$$I_{\omega_m}(t) \propto \cos\left(\frac{\beta'' L_2 \omega_m^{\,2}}{2M} \pm \frac{\pi}{4}\right) : \text{DSB single-arm with } V_{\pm b} \tag{12}$$

$$I_{\omega_m}(t) = const : \text{SSB with } V_{\pm b} \tag{13}$$

Fig. 3 shows the theoretical graph for the power penalty as a function of modulation frequencies in PTS system with M = 10. Again, as in the CW case, push-pull operation has only one power null while single-arm operation has two depending on the bias points. It can be seen that, for both SSB modulation and single-arm operation biased with V_{-b}, the PTS system incorporating with very high frequencies up to 40 GHz RF signals (which will be stretched down to lower frequencies up to 4 GHz with M = 10) do not suffer from the power penalty. On the other hand, the power degradation is severe for push-pull operation or single-arm operation biased with V_{+b} in this frequency range.

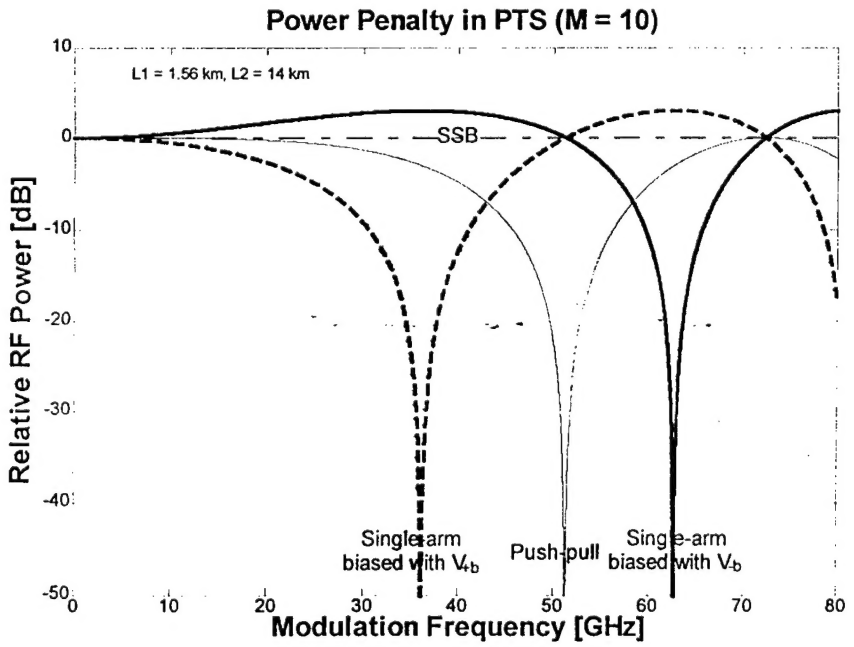

Fig.3 Power penalty as a function of modulation frequencies in PTS system with different modulation schemes and bias points for M = 10

IV. DEVICE FABRICATION AND EXPERIMENTAL SETUP

The SSB MZM structure of Fig. 1 was fabricated using the CPW1/APC polymer material. This guest-host system exhibited high EO coefficient, low material loss at 1.55 μm and good thermal stability [3]. New inverted rib waveguide structures were used for single-mode ridge waveguides, which provide enhanced confinement and much simpler fabrication procedure [4]. A large optical non-linearity in the core region was achieved through electrode poling. The microstrip lines were vertically aligned to the optical waveguides in the interaction regions to provide inherent velocity match of the RF signal and optical signal. The SSB modulator with the interaction length of 1 cm exhibited a DC V_π of 12 V.

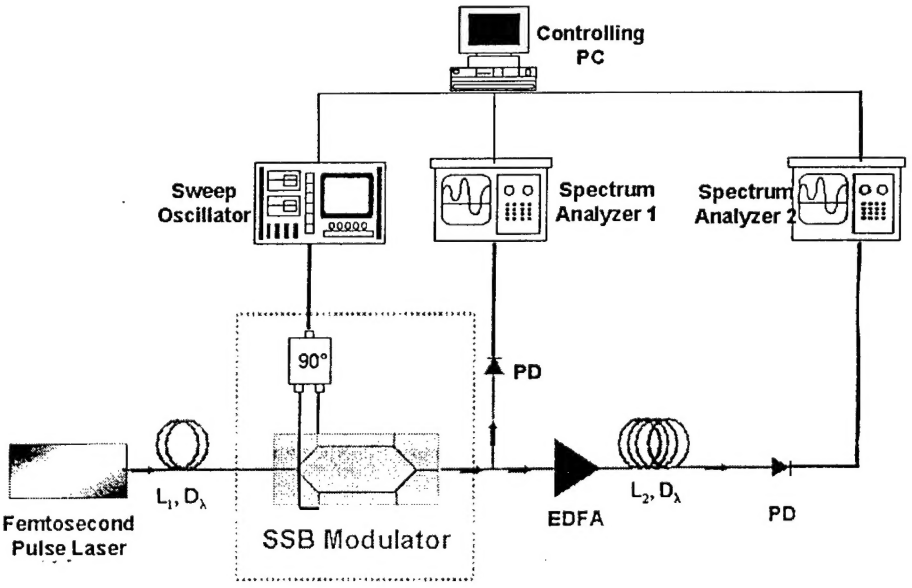

Fig.4 Block diagram of experimental setup for PTS (or CW measurement)

Fig. 4 shows the experimental setup for PTS (or CW measurement). The optical source is a pulsed Femtosecond laser system with a 40 nm bandwidth at 1.55 μm and a 40 MHz repetition rate (a 1.55 μm Er^{3+} fiber CW laser for CW measurement). Both fiber

spools L_1 and L_2 are standard SMF (L_1 = 0, $L2$ = 23 km for CW measurement). The dispersed input optical signal from L_1 is modulated at MZM by a 20 GHz sweep oscillator and amplified in an EDFA before entering L_2. The stretched output from the L_2 spool is detected by a 20 GHz bandwidth photodiode and amplified by 3–9 GHz RF amplifier. To exclude the frequency response of MZM, each RF power before and after L_2 are detected by two RF spectrum analyzers so that only RF power attenuation is measured as a function of modulation frequencies.

V. EXPERIMENTAL RESULT

1. Measurement with the CW Source

SSB modulation at 18GHz with the CW laser was first confirmed on the optical spectrum analyzer (OSA) at both bias voltages $V_{\pm b}$ to ensure the performance of our SSB modulators (Fig. 5).

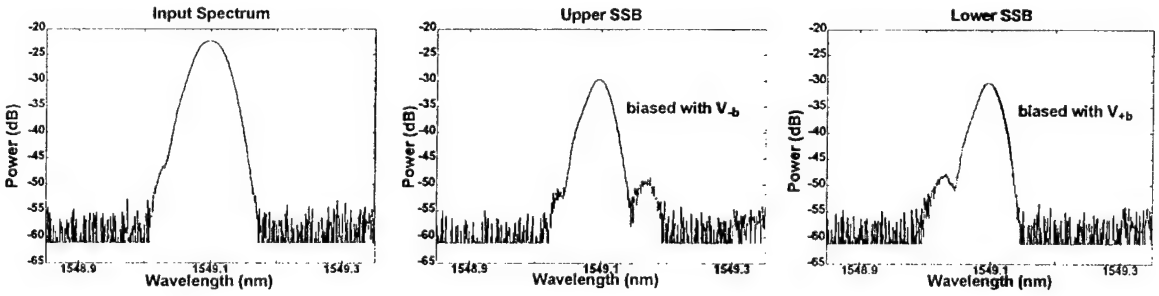

Fig.5 Measured optical SSB spectrum on OSA with a modulation frequency at 18 GHz

Fig. 6 shows the measured power penalty for various modulation schemes and bias points when the fiber length is 23 km. As expected in theory, DSB modulation driven by single-arm operation has different power nulls depending on the bias points. The bandwidth, when biased with V_{-b}, has been increased by amount of $\sqrt{3}$ compared to the another. For SSB modulation regardless of bias points, the power nulls have not been observed for the entire frequency ranges.

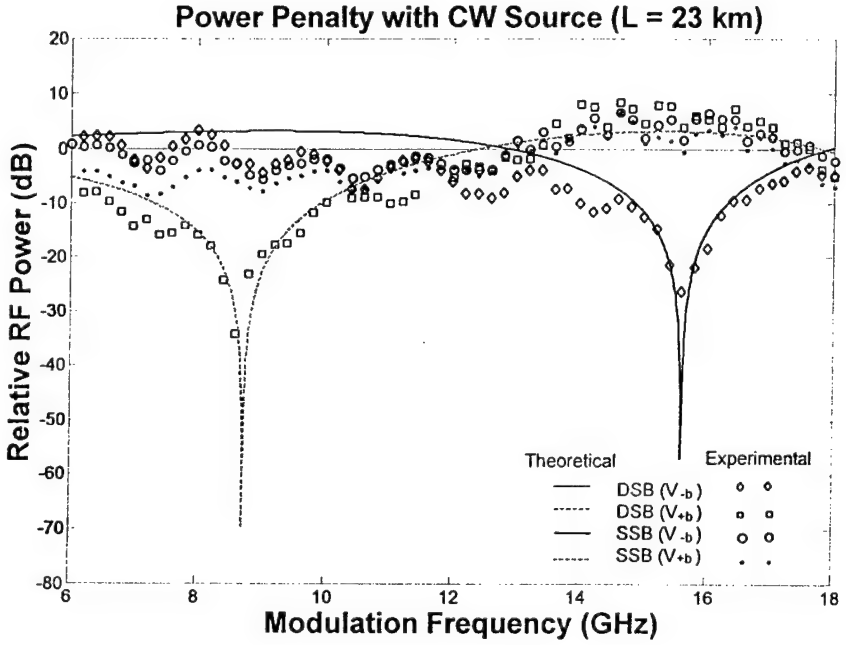

Fig.6 Measured power penalty for DSB and SSB modulation with different bias points (L = 23 km)

2. Measurement in PTS System

In our PTS measurement, RF signal was stretched from frequencies up to 18 GHz down to 9 GHz (M = 2.03). At each modulation frequency, the center of the shifted pulse spectrum is observed on the spectrum analyzer. Fig. 7 shows that measured time stretch ratio with fiber spools, L_1 = 13.6 km and L_1 = 14 km are in good agreement with the

theoretical value regardless of modulation conditions and bias points. Such a low M factor of 2 was intentionally used in our experiment to be able to see the first power nulls resulting from DSB modulation biased with $V_{\pm b}$ below the 20 GHz frequency range so that they can be easily compared at once. For bigger M both first power nulls associated with $V_{\pm}b$ would appear far beyond this frequency range.

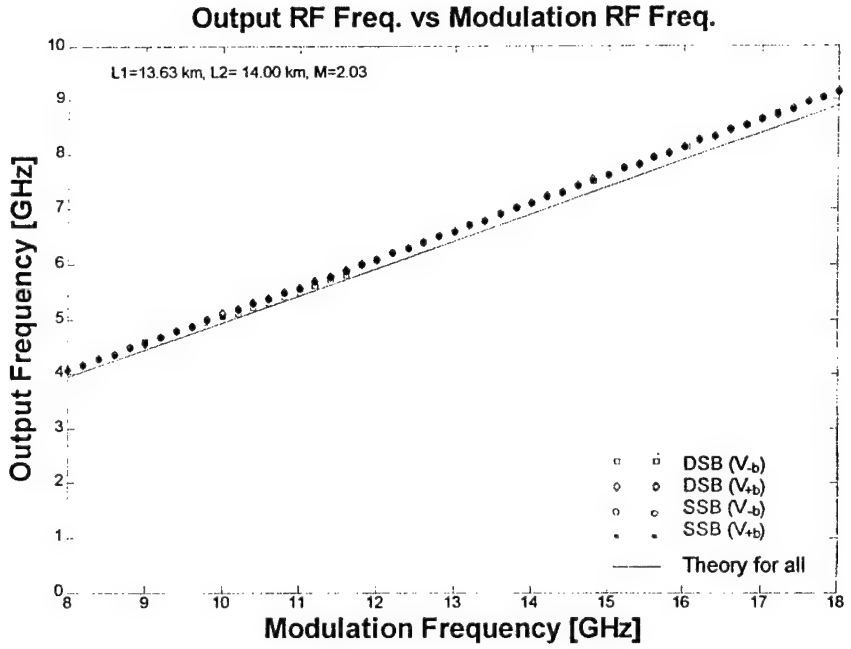

Fig.7 Measured time stretch ratio for DSB and SSB modulation with different bias points

The measured RF power penalties as a function of modulation frequencies for various modulation conditions are shown in Fig. 8. Also shown in Fig. 8 are the theoretical power penalties. As expected, DSB modulation biased at V_{+b} has the first power null at around 11.5 GHz while the DSB modulation biased at V_{-b} doesn't show the first power null below the frequency range of 18 GHz.. The limit on the modulation frequency due to the power penalty can be significantly improved even for DSB modulation by simply applying the alternative quadrature bias point. On the other hand, SSB modulation,

regardless of bias points, almost eliminates this penalty effect without bandwidth limitations as shown in Fig. 8.

Fig. 9 shows the RF power spectral density of modulated pulse before and after stretching for DSB modulation with two quadrature bias points, $V_{\pm b}$, at modulation frequency of 11.5 GHz. As expected from Fig. 8, the stretched RF signals at this modulation frequency exhibit considerable amount of power and almost zero power at quadrature bias point of V_{-b}, V_{+b}, respectively.

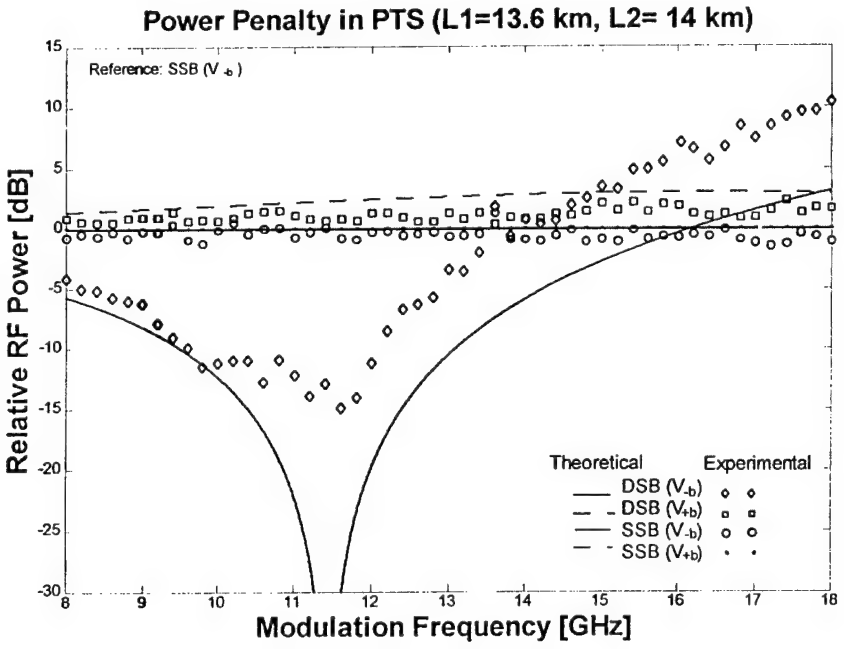

Fig.8 Measured power penalty in PTS system for various modulation schemes and bias points

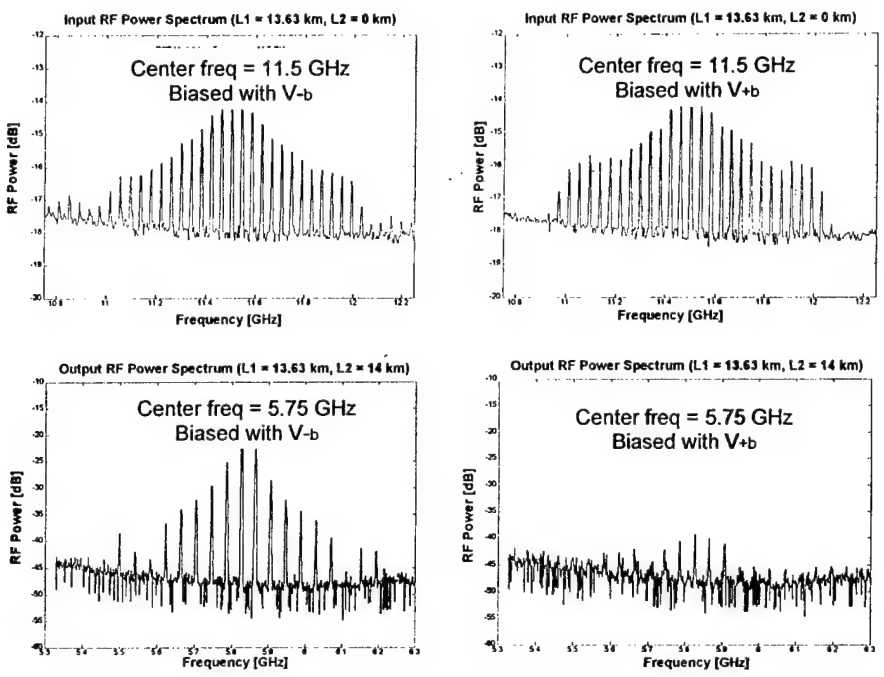

Fig.9 Measured input and stretched RF spectrums at different bias points for DSB modulation

VI. CONCLUSION

Photonic time-stretching has been demonstrated as a pre-processor to perform high-speed ADC of RF signals. Two techniques to reduce the power penalty due to fiber chromatic dispersion have been studied using our novel polymer modulators. High-frequency RF signal could be stretched down to lower frequency through the standard fiber without suffering this penalty by employing either SSB modulator configuration or a DSB modulator configuration with a alternative quadrature bias point.

REFERENCES

[1] Coppinger, F., Bhushan, A.S., Jalali, B., " Photonic time stretch and its application to analog-to-digital conversion" *IEEE Trans. on Microwave Theory and Tech.*, vol.47, no.7, p.1309-14, July 1999

[2] Chang, D.H., Erlig, H., Oh, M.C., Zhang, C., Steier, W.H., Dalton, L.R., Fetterman, H.R., "Time stretching of 102-GHz millimeter waves using novel 1.55 um polymer electrooptic modulator", *IEEE Photonics Technology Letters*, vol.12, no.5, p.537-9, May 2000

[3] Min-Cheol Oh, Hua Zhang, Cheng Zhang, Erlig, H., Yian Chang, Tsap, B., Chang, D., Szep, A., Steier, W.H., Fetterman, H.R., Dalton, L.R., "Recent advances in electrooptic polymer modulators incorporating highly nonlinear chromophore", *IEEE Journal of Selected Topics in Quantum Electronics*, vol.7, no.5, p.826-35, Sept./Oct.

[4] S. K. Kim, H. Zhang, D. Chang, C. Zhang, C. Wang, W. Steier and H. Fetterman, "Eelectro-optic polymer modulators with an inverted rib waveguide structure", *IEEE Photonics Technology Letters*, vol.12, no.5, p.537-9, May 2000

Time Stretching of 102-GHz Millimeter Waves Using Novel 1.55-μm Polymer Electrooptic Modulator

D. H. Chang, H. Erlig, M. C. Oh, C. Zhang, W. H. Steier, L. R. Dalton, and H. R. Fetterman

Abstract—**Millimeter (MM)-wave signals at frequencies up to 102 GHz have been time stretched down to 11 GHz using a new wide-band traveling-wave polymer modulator. This is the first application of electrooptic modulators fabricated using the new polymer material PC-CLD, which has demonstrated good optical insertion loss and high nonlinearity at 1.55 μm.**

Index Terms—**A/D conversion, electrooptic modulators, PC-CLD, photonic time stretch, polymer modulators.**

I. Introduction

THE ELECTROOPTIC modulator is an enabling component in many photonic and optical/millimeter (MM)-wave systems. As such, its bandwidth often dictates the range of applications which are feasible. Conventional $LiNbO_3$ modulators suffer from a large microwave to optical refractive index mismatch which limits their bandwidth. Polymer modulators have demonstrated promising high-frequency performance, with modulation response from dc out to 110 GHz [1]. Recently, modulators fabricated using the new polymer material PC-CLD have shown significantly reduced optical loss and high nonlinearity at 1.55 μm [2]. As an initial demonstration of its high-frequency capabilities, we have employed time stretch to detect modulation at frequencies up to 102 GHz. Time stretch utilizes linear group velocity dispersion in optic fibers to frequency downshift microwave signals modulated onto optical pulses. The technique has been proposed as a signal preprocessor to extend the upper frequency range of electronic analog/digital (A/D) converters, and has been demonstrated in [3].

Time stretch is related to frequency shifting of modulated optical pulses using time lenses [4], [5]. Time-lens action on electrical signals was also demonstrated earlier in [6]. Unfortunately, the authors of both [3] and [6] use the name "stretch," which can be a source of confusion. The fundamental difference between the two techniques is whether the temporal analog of the imaging condition is obeyed [7]. In [4]–[6], the imaging condition is fulfilled by the use of a quadratic phase (linear frequency) modulation element, which is the analog of a spatial thin lens. In the technique used in [3] and here, temporal magnification relies on dispersion alone. The spatial analog is simply a transparency held before a narrow beam, with the dispersive elements being the space between the beam source, the transparency, and the screen. This greatly simplifies implementation, but incurs a penalty which is analogous to that of an unfocused spatial imaging system. High frequencies are attenuated, imposing a bandwidth limitation which increases in severity with increasing magnification [3].

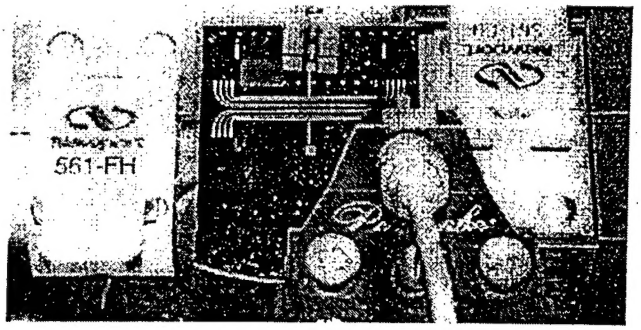

Fig. 1. PC-CLD polymer modulator in experimental setup with fiber coupling and V-band microwave probe. Light is coupled into and out of the modulator using fibers tipped with cylindrical lenses, which minimizes the coupling loss to about 1.5 dB/facet.

II. The PC-CLD Modulator

Fig. 1 shows the experimental unpackaged PC-CLD modulator used here. The substrate is gold-plated silicon, onto which the active material is spun and corona poled. Ridge optical waveguides are fabricated into the active material to form Mach–Zehnder interferometers (MZI's). The substrate serves as the ground plane for the microstrip lines patterned above the optical waveguides. Details on the fabrication and characterization of the device are discussed in [2]. The modulating electrical signal is injected from a coplanar probe near the input fiber. The probe shown is rated to 67 GHz; for modulation at 102 GHz, one with a W-waveguide input is substituted.

Figures of merit for the PC-CLD modulator are preliminary, as key elements such as interaction length and microstrip design are being optimized. Measurements conducted on this particular sample shows $V_\pi \approx 5$ V and total insertion loss of 12 dB. The device shows a flat frequency response to 40 GHz. Although operation well above 40 GHz has been demonstrated (for example in this experiment), a detailed frequency response measurement remains to be performed. While the device has survived repeated operation at 5–10 mW of optical power, long-term power limitations will be established once packaged units with fiber-pigtails are fabricated.

Manuscript received November 29, 1999; revised February 9, 2000. This work was supported under grants from the AFOSR and DARPA.

D. H. Chang and H. R. Fetterman are with the Department of Electrical Engineering, University of California at Los Angeles, Los Angeles, CA 90095 USA (e-mail: dhchang89@alum.mit.edu).

H. Erlig is with Pacific Wave Industries, Los Angeles, CA 90024 USA.

M. C. Oh, C. Zhang, W. H. Steier, and L. R. Dalton are with the Department of Electrical Engineering and Chemistry, University of Southern California, Los Angeles, CA 90098 USA.

Publisher Item Identifier S 1041-1135(00)03685-2.

III. Time-Stretch Theory

Time stretch exploits group velocity dispersion (GVD) to temporally expand a pulse while preserving its envelope shape. Details of the theory are in [3]. Two long fiber spools of length L_1 and L_2 are used, with the modulator in between. The relevant stretch factor M is the width of the pulse exiting L_2 compared to that exiting L_1. If we denote by τ_0 the pulse width exiting the laser and $\delta\tau_1$, $\delta\tau_2$ the additional broadening from L_1, L_2, respectively, then

$$M = \frac{\tau_0 + \delta\tau_1 + \delta\tau_2}{\tau_0 + \delta\tau_1} = 1 + \frac{\delta\tau_2}{\tau_0 + \delta\tau_1} \approx 1 + \frac{L_2}{L_1} \quad (1)$$

if $\tau_0 \ll \delta\tau_1$. This is certainly true in our system, where τ_0 (autocorrelation) $\approx$ 150 fs, while $\tau_0 + \delta\tau_1 > 1$ ns.

IV. Experimental Results

The optical source is a passively mode-locked Er^{3+}-doped fiber laser with a 50-nm pulse bandwidth at 1.55 μm and a 40-MHz repetition rate. To ensure linear propagation, the optical power is attenuated with a combination of neutral-density plates and variable attenuator. The output of the attenuator is propagated through L_1 (standard SMF) and a fiber-polarization controller before entering the modulator. The modulated output is amplified in an Er^{3+}-doped fiber amplifier before entering the L_2 spools, also SMF. The output of the L_2 spools is detected by a 45-GHz bandwidth photodiode and amplified by a 32-dB microwave amplifier. The specified passband of the amplifier is 8–12 GHz.

Four modulation sources are used: a sweep oscillator (to 40.8 GHz), a synthesizer (to 50 GHz), a GUNN oscillator (61.2 GHz), and a Klystron (102 GHz). Data are captured with both a spectrum analyzer and a sampling oscilloscope. To see the effect of time stretching directly in the time domain would require locking the laser pulse rate to the modulating source, an unavailable option for the last three sources. We instead rely on an indirect signature in the frequency domain, since the basic operation of time stretching has already been demonstrated [3]. The combined effect of modulation and subsequent time stretching is a frequency shifting of the carrier pulses' power spectral density to the stretched modulation frequency, which is observable using the spectrum analyzer.

Fig. 2 shows the unmodulated pulse after traversing the entire system, with $L_1 = 1.5$ and $L_2 = 4.5$ km. As can be seen, the pulse is much wider than its initial 150-fs width, and has acquired ripples which translate to "twin lobes" in the power spectral density. A fast Fourier transform (FFT) performed on the time-domain pulse corroborates the spectrum analyzer data. The source of the ripples has been isolated to the slight effective length mismatch between the two arms of the MZI. While such a mismatch is routinely compensated for with a bias voltage when modulating a CW beam, it produces intensity ripples in a highly chirped pulse. The ripple period is a function of the chirp parameter and the effective temporal mismatch. In addition, since waves of different polarizations in the optical waveguide suffer different mismatches, the overall output pulse shape is highly sensitive to the input polarization.

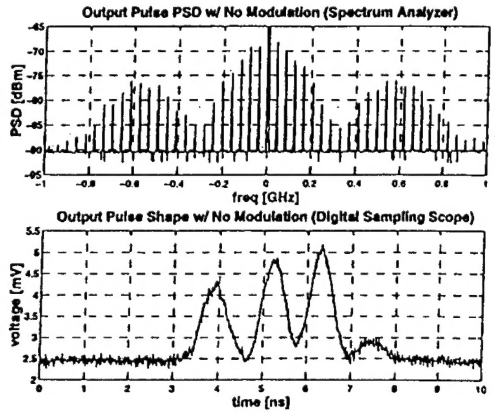

Fig. 2. Pulse power spectral density (PSD) and temporal shape with no modulation. The spike at dc is due to the noise floor.

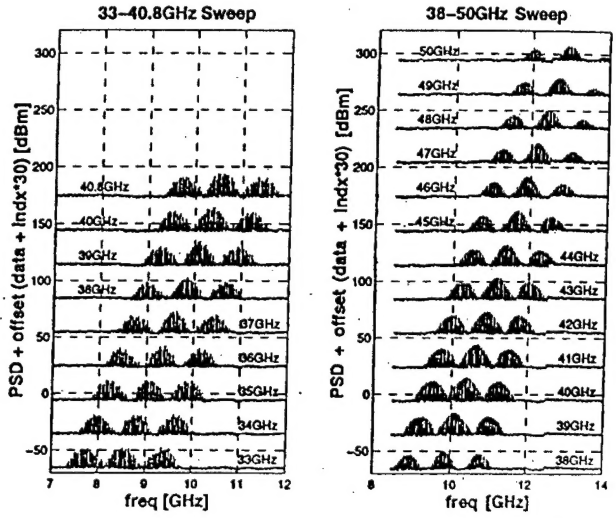

Fig. 3. Spectrum analyzer data for two modulation frequency sweeps. The spectra are replicas of that in Fig. 2 shifted to the stretched modulation frequency.

In an A/D application, the pulse ripples compete with the modulated signal and would be an undesirable feature which must be eliminated in postprocessing at the expense of conversion accuracy. For this experiment, no such compensation is required to recognize the effect of modulation, which simply frequency shifts the entire PSD waveform. The spacing between the PSD spectral lines is equal to the 40-MHz laser repetition rate, as expected.

Fig. 3 shows the shifted spectra as the modulation frequency is swept from 33 to 50 GHz, with $L_1 = 1.5$ and $L_2 = 4.5$ km. The centers of the captured spectra are extracted and plotted against the modulation frequency in Fig. 4. As expected, the relationship is linear; the fitted M is 3.86. The "upper lobes" of the spectra near 50 GHz are distorted by the bandwidth of the 8–12-GHz microwave amplifier.

In Fig. 5, a GUNN oscillator with a measured peak at 61.8 GHz is used to drive the modulator. To bring the stretched waveform back into the microwave amplifier's passband, L_2 is increased to 6.5 km, while L_1 remains at 1.5 km. In all other aspects, the system remains unchanged from the 33- to 50-GHz data set. The measured M is 5.13.

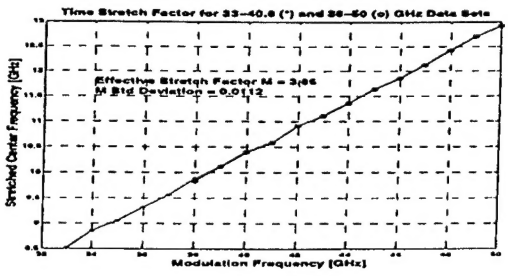

Fig. 4. Effective stretch ratio calculated for data sets seen in Fig. 3. From the data, $M_{eff} = 3.86$, with a 1σ deviation from linearity of 1.1%. The calculated value from (1) is $M = 4$.

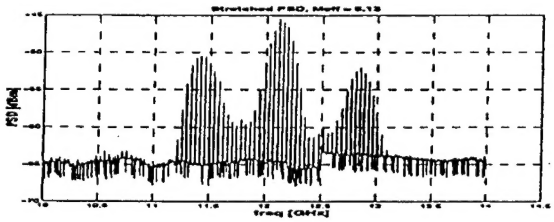

Fig. 5. GUNN-oscillator source with output measured at 61.81 GHz is time stretched to 12.05 GHz ($M = 5.13$). The pulse shape remains similar to that in Fig. 3.

Finally, time stretch using a Klystron oscillator at 101.7 GHz (as measured by a frequency counter and harmonic mixer) is shown in Fig. 6. Now $L_1 = 0.5$ and $L_2 = 5.0$ km to bring M to 11; the measured ratio is 9.8. The large change in fiber arrangement alters the pulse shape, as can be inferred by the zero-modulation PSD in Fig. 6. With the signal level available, only the top portion rises above the noise floor in the stretched data.

The discrepancies between measured and calculated stretch ratios stem from dispersion introduced ahead of the modulator by the variable attenuator and a 50-m fiber patch cord connecting the laser to the L_1 spool. The effective M from (1) is

$$M_{\text{eff}} = 1 + \frac{L_2}{L_1 + \delta}$$

where δ represents dispersion equivalent to that length of SMF. Solving for δ in the three frequency regimes using measured M_{eff}'s of 3.86, 5.13, and 9.80 gives self-consistent values of 73, 74, and 68 m, respectively.

V. Conclusion

This experiment is the first reported application of electrooptic modulators fabricated from the new polymer material PC-CLD. We have utilized time stretching to show modulation at up to 102 GHz. It extends the previously demonstrated high-frequency capabilities of polymer modulators to important 1.55-μm applications.

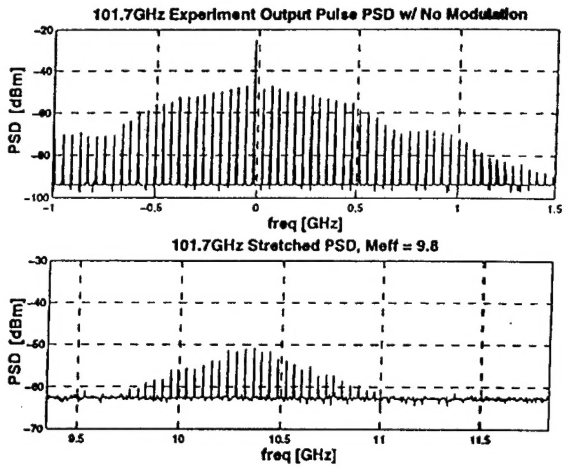

Fig. 6. Stretch experiment with 101.7-GHz Klystron source. Top trace is zero-modulation spectrum, differing slightly from Fig. 2 because increasing M from 4 to 11 has changed the pulse shape. Bottom trace shows stretched spectrum with $M_{eff} = 9.8$. The frequency axes for both plots have the same scaling and span.

It must be noted that time stretching suffers an inherent bandwidth limitation, analogous to defocused imaging in the spatial domain. As calculated in [3], the intensity transmission versus modulation frequency consists of a series of deep notches; a larger M results in a lower first-notch frequency. For this experiment, the narrow-band modulation signals were chosen to avoid the notch frequencies, an unavailable option for a wide-band signal. In an A/D preprocessor application, the actual system bandwidth is limited both by the modulator and the maximum stretch ratio required to map into the A/D converter's operating range.

Acknowledgment

The authors would like to thank I. Poberezhskiy, Drs. B. Tsap and Y. Chang, H. Zhang, Drs. F. Coppinger and B. Jalali, and A. S. Bhushan for their assistance.

References

[1] D. Chen, H. R. Fetterman, A. Chen, W. H. Steier, L. R. Dalton, W. Wang, and Y. Shi, "Demonstration of 110 GHz electro-optic polymer modulators," *Appl. Phys. Lett.*, vol. 70, no. 25, pp. 3335–3337, 1997.

[2] M. C. Oh, H. Zhang, A. Szep, V. Chuyanov, W. H. Steier, C. Zhang, and L. R. Dalton, "Practical electro-optic polymer modulators using PC/CLD," in *Organic Thin Films for Photonic Applications*, Sept 1999.

[3] F. Coppinger, A. S. Bhushan, and B. Jalali, "Photonic time stretch and its application to analog-to-digital conversion," *IEEE Trans. Microwave Theory Tech.*, vol. 47, no. 7, pp. 1309–1314, 1999.

[4] C. V. Bennett and B. H. Kolner, "Upconversion time microscope demonstrating 103X magnification of femtosecond waveforms," *Opt. Lett.*, vol. 24, no. 11, pp. 783–785, June 1999.

[5] C. V. Bennett, R. P. Scott, and B. H. Kolner, "Temporal magnification and reversal of 100 Gb/s optical data with an up-conversion time microscope," *Appl. Phys. Lett.*, vol. 65, no. 20, pp. 2513–2515, Nov. 1994.

[6] W. J. Caputi, "Stretch: A time-transformation technique," *IEEE Trans. Aerosp. Electron. Syst.*, vol. AES-7, pp. 269–278, March 1971.

[7] B. H. Kolner, "Space–time duality and the theory of temporal imaging," *IEEE J. Quantum Electron.*, vol. 30, pp. 1951–1963, Aug. 1994.